Journal of Catalysis 262 (2009) 188–198

Contents lists available at ScienceDirect

Journal of Catalysis

www.elsevier.com/locate/jcat

Modified cobalt catalysts in the partial oxidation of methane at moderate temperatures

Bjørn Christian Enger [a], Rune Lødeng [b], Anders Holmen [a,*]

[a] Department of Chemical Engineering, Norwegian University of Science and Technology (NTNU), N-7491 Trondheim, Norway
[b] SINTEF Materials and Chemistry, N-7465 Trondheim, Norway

ARTICLE INFO

Article history:
Received 19 September 2008
Revised 24 November 2008
Accepted 12 December 2008
Available online 23 January 2009

Keywords:
Synthesis gas
Partial oxidation
Activation
Dissociation
Pyrolysis
Methane
Cobalt
Alumina

ABSTRACT

Cobalt on alumina catalysts were prepared and tested in the partial oxidation of methane using dry feed at moderate gas temperatures (700–973 K) and atmospheric pressure. The effect of adding small amounts (1/15 molar ratio) of Ni, Fe, Cr, Re, Mn, W, Mo, V and Ta oxides was studied. The catalysts were prepared using incipient wetness impregnation followed by direct reduction of catalyst precursors, and characterized using H_2 chemisorption, N_2 sorption, TPx, XRD and XPS. The catalytic testing was performed using air as oxidant with $CH_4/O_2 = 2$ and a gas hourly space velocity of 15–150 Nl CH_4/(g h). The product composition was compared to thermodynamic equilibrium at bed exit temperatures, and any deviation from equilibrium could be explained by temperature gradients. It was found that the presence of co-impregnated metals or metal oxides that may either form bimetallic or mixed oxide species with cobalt was detrimental to the catalyst performance. The most detrimental elements included Mo, W, V and Ta, and their poor activity for synthesis gas formation could be explained by the low cobalt metal surface area determined from hydrogen chemisorption, as compared to the unmodified catalyst. Results indicate that deactivation of cobalt involves oxidation of the active phase, and that carbonaceous deposits may be involved in the deactivation. When increasing the gas hourly space velocity the presence of a modifier had a dramatic effect on the catalyst performance, and only Ni improved catalyst stability and yields. All other modifications tested were detrimental to methane conversion at the levels investigated. Dissociation of methane was investigated by TPx, and the activation of C–H bonds was found to occur above the hcp to fcc phase transition temperature of cobalt, indicating that methane activation to synthesis gas could be structure sensitive on metallic cobalt. A 2–3 zone reaction mechanism involving pyrolysis, combustion and reforming is suggested.

1. Introduction

The production of synthesis gas has been studied since the beginning of the 20th century, and different approaches to synthesis gas and hydrogen production have been reviewed on a regular basis [1–3].

CO_2 handling is a growing research topic, and the prospects range from sequestration to utilization in the production of chemicals [4]. In this context, oxidative concepts like catalytic partial oxidation (CPO) and autothermal reforming (ATR) seem attractive for a number of reasons, such as efficient use of raw materials, low energy demand and the potential of operation at high space velocity in compact reactors [5]. Compared to CO_2 capture from internal combustion, where typically only 3–4 vol% of the exhaust gas is CO_2, synthesis gas production followed by water–gas shift, utilizing permselective membranes to remove hydrogen, would yield highly concentrated CO_2 for sequestration, and H_2 which could be used in fuel cell applications.

Partial oxidation of methane is a well-known reaction with theoretical and experimental studies dating back to Liander [6] and Prettre et al. [7]. The history of catalytic partial oxidation of methane is rather extensive, even though the major body of scientific contributions originated after the studies by Ashcroft et al. [8,9] and Hickman and Schmidt [10]. Catalytic partial oxidation of methane has been reviewed on a regular basis [5,11–17], and a general review, with the exception of a few key points, is therefore unnecessary in this context.

The 'direct' route in CPO, given by reaction (1),

$$CH_4 + (1/2)O_2 \rightarrow CO + 2H_2, \quad \Delta H^0_{298\ K} = -35.7\ \text{kJ/mol}, \tag{1}$$

is in principle ideal for the production of hydrogen or synthesis gas for gas-to-liquid applications. The oxidation of methane is practically irreversible at all temperatures under atmospheric conditions.

* Corresponding author.
E-mail address: anders.holmen@chemeng.ntnu.no (A. Holmen).

0021-9517/$ – see front matter
doi:10.1016/j.jcat.2008.12.014

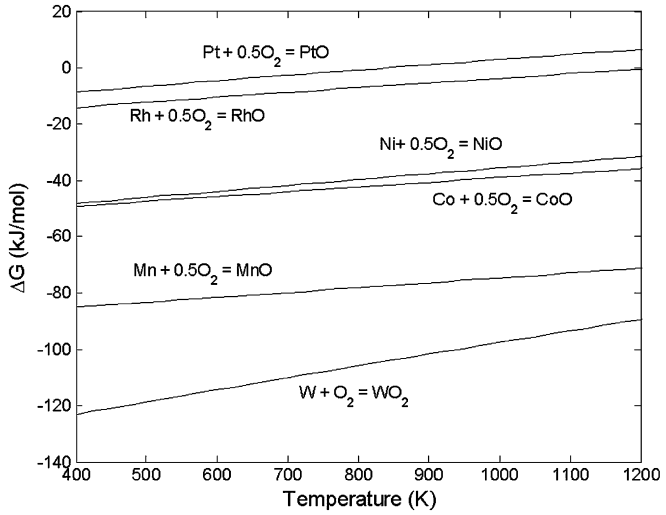

Fig. 1. Illustration of the change in Gibbs free energy for the oxidation of Co, Ni, Rh and Pt as a function of temperature, calculated using HSC Chemistry 5.1.

However, it is typically observed that other overall reactions, including combustion, reforming and shift, play important roles, effectively limiting the yields by a global thermodynamic equilibrium. The more favoured combustion reaction (2) typically creates a distinctive bed-temperature gradient which complicates the measurements of intrinsic kinetic parameters:

$$CH_4 + 2O_2 \rightarrow CO_2 + 2H_2O, \quad \Delta H^0_{298\ K} = -802.3\ \text{kJ/mol}. \qquad (2)$$

H_2 and CO are the thermodynamically favoured products at high temperatures (>1273 K), and it has been shown by Hickman and Schmidt [18] that equilibrium can be obtained in an autothermal short-contact time reactor. However, commercialization of the process at these temperatures will require expensive reactor materials. Different straight low chromium and austenitic stainless steel materials (i.e. type 316) have an upper limit of about 1143 K for intermittent service or 1198 K for continuous service in air [19]. Catalyst stability is also a critical issue at these temperatures. It is therefore desirable to conduct production of synthesis gas at lower temperatures, typically <1073 K.

The use of cobalt catalysts in methane partial oxidation has recently been reviewed [17,20]. Cobalt has a strong tendency to be oxidised at lower temperatures, as easily verified by thermodynamic calculations as a function of temperature and illustrated for Co, Ni, Pt, Rh, Mn and W in Fig. 1, and a promoter may therefore be beneficial to keep it partially reduced. Lødeng et al. [20] investigated the effect of different transition metals including Ni, Pt, Rh, Ru and Pd. The addition of Pt and Rh was found to be beneficial for maintaining activity at low temperatures, while Ni promoted carbon formation and deactivation. No clear effects of Pd or Ru were observed. Pt has previously been reported to promote the reduction of cobalt [21] leading to higher yields of synthesis gas [22,23].

The scope of the presented work was to study the effect of modifying cobalt catalysts with a second metal oxide when tested in the partial oxidation of methane. The idea behind this was to try to investigate whether the cobalt crystals were decorated, covered or encircled by a second phase and to what extent this affected catalyst performance. The modifiers in this study was largely based on the principle that in any chemical process it may be just as important to identify groups of elements that have negative effects as identifying the best promoters.

Catalysts with similar average particle sizes were prepared on an inert support and characterized by different methods including H_2 chemisorption, XRD, TPx and XPS. The catalysts were subsequently tested for activity at moderate temperatures using dry feed. Properties including the available cobalt surface area, particle sizes, and the nature of the cobalt and second metal or metal oxide phases have been addressed.

Table 1
Catalyst properties on α-Al_2O_3 (18.5 m^2/g).

Catalyst ID	Co (wt%)	M (wt%)	$H_{2,diff}$[a] (H:Co)	$H_{2,tot}$[b] (H:Co)	$t_{XRD}^{Scherrer}$ (nm)	$t_{XRD}^{Mapping}$[c] (nm)
Co	14.2	0	0.016	0.033	17.1	16.1 ± 0.6
Ni/Co	14.0	0.9	0.011	0.022	18.3	17.7 ± 0.5
Fe/Co	14.0	0.9	0.009	0.016	16.7	16.5 ± 0.6
Cr/Co	14.1	0.8	0.008	0.017	15.1	12.3 ± 0.4
Re/Co	13.8	2.9	0.006	0.016	16.2	14.5 ± 0.9
Mn/Co	14.0	0.9	0.006	0.015	15.0	16.1 ± 0.7
W/Co	13.8	2.9	0.003	0.010	15.7	17.1 ± 0.6
Mo/Co	14.0	1.5	0.003	0.008	17.6	16.5 ± 0.7
V/Co	14.1	0.8	0.000	0.000	16.0	18.0 ± 0.5
Ta/Co	13.8	2.8	0.000	0.000	17.8	18.9 ± 0.6

[a] The difference between first and second adsorption isotherm of H_2 adsorption at 373 K. Sometimes referred to as the irreversible adsorption (chemisorption).
[b] Total H_2 adsorption at 373 K.
[c] The mapping is done with DIFFRACPlus Powder v.1.07, and the thickness is the Scherrer thickness calculated from the FWHM of the peaks.

2. Experimental

2.1. Catalyst preparation

The catalyst support was prepared from γ-Al_2O_3 (190 m^2/g), which was calcined to a surface area of 18.5 m^2/g by heating at 10 K/min from ambient to 1298 K followed by 2 K/min 1298–1398 K and 10 h at 1398 K. The support was cooled from 1398 K to ambient inside the oven over a period of 10 h.

The cobalt catalysts were prepared by incipient wetness impregnation using a watery solution of cobalt nitrate hexahydrate $Co(NO_3)_2{\cdot}6H_2O$, and a molar ratio of Al/Co = 7 corresponding to 14.2 wt% Co/Al_2O_3 before adding the modifier. After drying for 1 h at 383 K the modifier percursors were added by incipient wetness impregnation from the following precursors. $Ni(NO_3)_2{\cdot}6H_2O$, $Fe(NO_3)_2{\cdot}9H_2O$, $Cr(NO_3)_3{\cdot}9H_2O$, $HReO_4$ (77.5% Re aq. solution), $Mn(NO_3)_2{\cdot}6H_2O$, H_2WO_4, $H_2MoO_4{\cdot}H_2O$, V_2O_5 and $TaCl_5$. The precursors were added with molar ratios Co/M = 15, where M is the second metal.

The nitrate precursors were all added using a watery solution, while the W, Mo, V and Ta precursors are insoluble in water. In order to avoid using alkaline solutions containing either K or Na for H_2WO_4, $H_2MoO_4{\cdot}H_2O$ and V_2O_5, or a carbon based solvent such as ethanol for $TaCl_5$, the fine powders were mortared and physically mixed with the cobalt impregnated catalyst before dropwise addition of water was added to reach the incipient wetness point. The purpose of this procedure was that the ultrafine powdery precursors would be sucked into the catalyst pores by capillary forces. The reason for avoiding K or Na was that these are known promoters that were expected to modify the catalyst properties [20,24] and ethanol could potentially leave a carbon based residue on the catalyst during direct reduction at elevated temperatures.

Direct reduction of catalyst precursors was carried out in a quartz reactor at 823 K (4 h) with 50 Nml H_2/min in 100 Nml He/min. Heating at 10 K/min from ambient to 773 K was followed by 2 K/min from 773 to 823 K before 4 h steady reduction at 823 K, and subsequently cooled to ambient. Table 1 shows the catalyst compositions ordered by the adsorption ratio H/Co.

2.2. Partial oxidation of methane

Catalytic partial oxidation was carried out in co-feed modus in a quartz reactor at atmospheric pressure. The tubular reactor

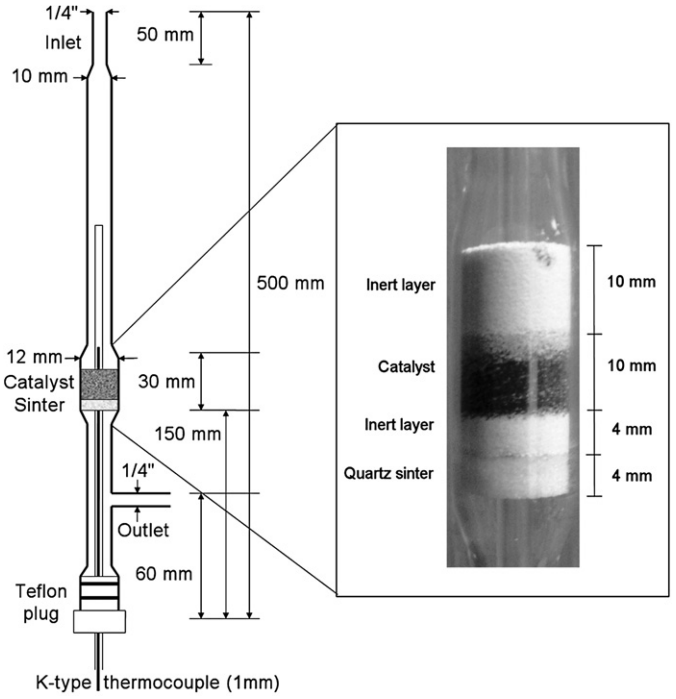

Fig. 2. Schematic illustration of the tubular quartz reactor (12 mm i.d.) containing a closed-end internal axial quartz tube (4 mm o.d.) equipped with a movable K-type thermocouple (1 mm) enabling the measurements of gas temperatures (left). Enlarged image of the catalyst bed (right) and inert α-Al_2O_3.

(12 mm i.d.) contained an axial quartz tube (4 mm o.d.) equipped with a movable thermocouple for apparent gas temperature measurements. Fig. 2 shows the reactor with catalyst and inert material. The reactor was placed inside an electrically heated gold insulated furnace (Thermcraft Trans Temp) giving an isothermal profile in the absence of reaction. The bed exit gas temperatures and gas hourly space velocities were typically in the range 573–973 K and 15–150 Nl CH_4/(g h), respectively. The catalyst particles (<0.1 mm) were diluted with inert material (α-Al_2O_3) of a similar size and pre-reduced in 30 Nml H_2/min by heating at 10 K/min from ambient to 923 K, followed by 2 h reduction at 923 K.

Product analysis was carried out by gas chromatography (Agilent G2891A MicroGC) using a thermal conductivity detector (TCD) and two columns: (A) Molecular Sieve 5 Å with carrier gas Ar, (B) PoraPLOT U with carrier gas He. Total concentrations calculated by multiple non-linear calibration points typically added up to $99.0 \pm 1.0\%$, indicating good overall consistency, while carbon mass balances where typically consistent to $96.0 \pm 1.0\%$. This discrepancy was an artifact caused by the carbon mass balance closure using N_2 as internal standard. It was found that the measured CH_4/N_2 ratio was not independent of the total flow of these two species even though the mass flow controller (MFC) calibration lines were exceptionally good ($R^2 \cong 0.999 \pm 0.001$). It was concluded that this artifact was caused by properties related to the sampling of the GC and not a real closure problem in the mass balances of the system.

The conversion X of methane, and selectivities S to H_2 and CO were calculated by the following equations based on normalized gas concentrations:

$$X_{CH_4} = \frac{y_{CH_4}}{\sum_{j=1}^{n} j y_{C_j}}, \tag{3}$$

$$S_{CO} = \frac{y_{CO}}{y_{CH_4}} X_{CH_4}, \tag{4}$$

$$S_{H_2} = \frac{y_{H_2}}{2((\sum_{j=1}^{n} j y_{C_j}) - y_{CH_4})} = \frac{y_{H_2}}{2y_{CH_4}} \left(\frac{X_{CH_4}}{1 - X_{CH_4}} \right), \tag{5}$$

where y_i are the gas concentrations in product stream. The denominator in the expression for conversion is the carbon mass balance.

2.3. Methane dissociation

The activation of methane was investigated over Co/α-Al_2O_3 by temperature-programmed methane dissociation (TPMD) using the micro GC for rapid sampling. The catalyst (0.20 g) was placed on top of α-Al_2O_3 (0.40 g) and pre-reduced in 30 Nml H_2/min by heating at 10 K/min from ambient to 923 K, followed by 2 h reduction at 923 K. After cooling to room temperature the catalyst was exposed to a feed consisting of 20 Nml CH_4/min in 500 Nml N_2/min, and heating was carried out from ambient to 1073 K at 5 K/min. Temperature-programmed oxidation (TPO) of dissociated methane was carried out subsequently using a feed consisting of 50 Nml air/min in 500 Nml N_2/min. The temperature was increased from ambient to 1073 K at 5 K/min.

2.4. Catalyst deactivation

Following catalytic partial oxidation of methane over Co/α-Al_2O_3, both active and deactivated samples were tested by *in situ* temperature-programmed reduction (TPR) using the micro GC for rapid sampling of the H_2 signal. The catalyst (0.20 g) was placed on top of α-Al_2O_3 (0.40 g). The feed consisted of 10 Nml H_2/min in 500 Nml N_2/min, and the temperature was increased from ambient to 973 K at 5 K/min.

2.5. Surface area measurements with N_2 or H_2

Isotherms from volumetric adsorption and desorption of nitrogen were measured at the boiling point of liquid nitrogen using a standard commercial equipment (Micromeritics Tristar 3000). The sample (0.70 g) was placed in the quartz container, vacuum dried at 573 K for 1 h and cooled to room temperature before the measurements. The surface area was calculated using the BET [25] and the BJH [26] methods. The BJH method applied assumed a slit pore shape and stepped off the desorbed volume by using the Kelvin equation and a film thickness equation.

Isotherms from volumetric chemisorption of hydrogen were measured at 373 K in an apparatus (Micromeritics ASAP 2010) at a pressure of $<10^{-3}$ Pa. The sample (0.40 g) was placed in a U-tube quartz reactor, dried and evacuated at 313 K and reduced in flowing hydrogen for 2 h at 923 K. The sample was evacuated and cooled to 373 K before chemisorption isotherms were obtained. The hydrogen to metal ratio H/M was calculated using Eq. (6):

$$\mathrm{H/M} = C_t \frac{M_M}{x_M}, \tag{6}$$

$C_t = V_{ads}/22711$ is the total concentration of sites (mol/g), where V_{ads} was obtained from an extrapolation of the linear part of the isotherm to zero pressure, 22711 (Ncm^3/mol) is the ideal gas volume at 1 bar and 273 K. x_M is the mol fraction of metal M and M_M is the molar mass of metal M.

2.6. Temperature-programmed methods (TPx)

Temperature-programmed reduction (TPR) and oxidation (TPO) was carried out in a U-tube quartz reactor. The sample (0.20 g) was placed in an insulated furnace and heated from ambient to 1010 K at 10 K/min in a stream of 30 Nml/min 5% O_2 in Ar. After cooling to ambient the sample was flushed with 30 Nml/min Ar for 30 min before it was heated from ambient to 1210 K at 10 K/min in a stream of 30 Nml/min 7% H_2 in Ar. The O_2 or H_2 consumption was measured from the effluent gas by a thermal

conductivity detector (TCD). The apparatus has been described in detail elsewhere [27].

2.7. X-ray photoelectron spectroscopy (XPS)

X-ray photoelectron spectra were obtained using a hemispherical SES-2002 electron energy analyzer (GammaData Scienta). A monochromatized AlK_α (1486.6 eV) X-ray source (GammaData Scienta) was used for the excitation. The total energy resolution was about 0.7 eV as determined from the width of the Fermi edge. The samples were crushed, mounted on carbon paper pads and measured in angle integrated mode around normal emission.

2.8. X-ray diffraction (XRD)

X-ray diffraction spectra were obtained using a Siemens D5005 X-ray diffractometer with monochromatic CuK_α radiation. The results were used to calculate particle diameters of metallic cobalt and CoO using the Scherrer equation [28], and by using Gaussian mapping in the software package DIFFRACPlus Powder v.1.07.

3. Results and discussion

3.1. Heat and mass transport

Considering the exothermicity of reactions relevant to CPO, heat removal from the catalyst may be an issue, as illustrated by several studies where IR thermography was used [29–34]. The presence of internal or external diffusional limitations may be addressed by the Weisz–Prater [35] and Mears [36] criteria, respectively. However, it has been illustrated by spatially resolved profiles, for example of a Rh foam [37–39], that the conversion of oxygen and methane is typically extremely rapid at the bed entrance, where about 70–100% of the oxygen is consumed within 1 mm of the 10 mm catalyst bed. Even though the spatial profiles are likely different for these cobalt catalysts where air was used as oxidant, applying the overall reaction rate to the Weisz–Prater and Mears criteria substantially underestimates the actual reaction rate at the bed entrance, and correspondingly underestimates the potential for diffusional limitations. To correctly estimate the potential for diffusional limitations, such criteria need to be applied to differential segments of the catalyst bed using spatially resolved profiles for the calculation of reaction rates. However, such spatially resolved profiles were not obtained in this study.

In the absence of spatially resolved profiles, in order to obtain a rough estimate of possible external diffusional limitations, the Mears criterion given by Eq. (7) was calculated assuming 50% O_2 conversion within 1 mm of the bed:

$$N_{\text{Mears}} = \frac{-r_A \rho_b R n}{k_c C_{bA}} < 0.15, \tag{7}$$

where r_A is the rate of reaction (mol/(g s)), ρ_b is the bulk density of the catalyst bed (g/cm^3), R is the particle size (m), n is the reaction order, k_c is the film mass transfer coefficient (m/s) and C_{bA} is the bulk concentration of A (mol/cm^3). Diffusional limitations only occur when $k_c < u_0$, where u_0 is the linear bulk fluid velocity. An upper limit may therefore be calculated using u_0 in place of k_c. Using this and assuming the reaction order of oxygen to be in the range 0.5–2, according to reaction stoichiometrics for partial oxidation and total combustion, it was found that N_{Mears} was in the range 1.5–6.3 for a gas temperature of 1000 K at our highest gas velocity (0.07 m/s). This indicates strong mass transfer limitations on oxygen in all our studies. The same conclusion was reached for methane assuming 30% conversion of methane within 1 mm of the bed. The actual N_{Mears} numbers are likely higher, since as already mentioned, the bulk linear velocity u_0 was used in place of k_c.

According to Froment and Bischoff [40] a simple way to estimate the maximum possible temperature difference between the surface and gas phase $T_s - T$ is using Eq. (8):

$$(\Delta T)_{\max} = 0.7\left[\frac{-\Delta H}{M_m c_p}\right]\left[\frac{\ln(1+\delta_A p_A/p_t)}{\delta_A}\right]. \tag{8}$$

Here ΔH is the reaction enthalpy, M_m and c_p are, respectively, the molar mass and heat capacity of the fluid and p_A is the partial pressure of A in the feed. Assuming only partial oxidation is taking place, which is mildly exothermic with $\Delta H = -25.9$ to -22.6 kJ/mol in the temperature range 673–1273 K, $(\Delta T)_{\max}$ was found to be 48–66 K. However, considering the exothermicity of total combustion with $\Delta H \approx 800$ kJ/mol and taking into account the selectivity, ΔH was calculated to be about 120 kJ/mol for the overall reactions. This corresponds to a $(\Delta T)_{\max}$ in the range 250–300 K, and a maximum surface temperature not exceeding 1330 K:

Comparing our estimate to some literature values, Bizzi et al. [41] reported a temperature difference between maximum surface temperature and outlet gas temperature in the range 388–422 K for rhodium coated alumina. Chang and Heinemann [42] reported maximum temperatures in the range 1474–1573 K when studying 28 wt% Co/MgO, however, in their case the mixture was methane and pure oxygen.

For rhodium supported on alumina the CPO process can be roughly divided into 2–3 zones. At the reactor inlet high oxidation states are present with correspondingly high probabilities for complete combustion, and the reactor outlet with low or zero valent oxidation states and correspondingly higher probabilities for reforming reactions. These two distinctly different zones are separated by a narrow transition region where the oxidation state changes rapidly as a function of the vertical position in the bed [43]. It is highly probable that similar 2–3 zones with changing oxidation states of the catalyst are present also for other reducible catalysts during CPO, including our cobalt catalysts. An exception to this could be platinum, which according to Fig. 1 is difficult to oxidise at high temperatures once present in the metallic state.

3.2. Steady-state CPO

Table 2 summarizes the results from steady-state partial oxidation at low GHSVs. It shows that modifying the available cobalt surface area with a second metal or metal oxide has no apparent effect on the selectivity or conversion level when these are

Table 2
Steady-state activity and *ex-situ* characterization data.

Catalyst ID	$H_{2,diff}$[a] (H:Co)	BJH SA[b] (m^2/g)	BJH PV[c] (ml/g)	X_{CH_4}[d] (%)	S_{H_2} (%)	S_{CO} (%)
Co	0.016	18.5	0.065	74_s	90	86
Ni/Co	0.011	19.2	0.070	73_s	89	85
Fe/Co	0.009	19.2	0.071	$57_\downarrow$	80	71
Cr/Co	0.009	22.5	0.083	74_s	90	86
Re/Co	0.006	20.2	0.070	75_s	90	86
Mn/Co	0.006	21.0	0.072	74_s	90	86
W/Co	0.003	21.6	0.076	$14_\downarrow$	1	5
Mo/Co	0.003	21.8	0.079	$7_\downarrow$[e]	2	12
V/Co	0.000	19.5	0.074	$20_\downarrow$	1	7
Ta/Co	0.000	19.1	0.072	$17_\downarrow$	1	2

[a] The difference between first and second adsorption isotherm of H_2 adsorption at 373 K. Sometimes referred to as the irreversible adsorption (chemisorption).
[b] Barrett–Joyner–Halenda surface area [26].
[c] Barrett–Joyner–Halenda pore volume [26].
[d] Subscript s indicate steady-state while ↑ or ↓ indicate increasing or decreasing values. GHSV = 15 Nl CH_4/(g h), CH_4:O_2:N_2 = 2:1:3.72, T_{furnace} = 923 K, values are after 2 h on-stream.
[e] After only 1 h on-stream.

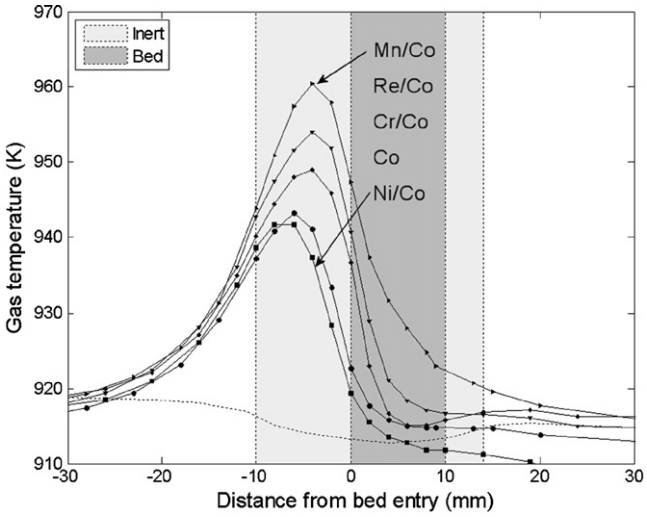

Fig. 3. Temperature profiles from the partial oxidation of methane with air (CH_4/O_2 = 2.0) at 923 K (oven temperature) and GHSV = 15 Nl CH_4/(g h). Steady state was kept for 2 h before the oven temperature was decreased with 1 K/min. The catalysts are indicated in order of appearance based on the peak maximums.

within experimental error of the equilibrium values at bed exit gas temperatures. The presence of elements that likely will remain unreduced oxides, or form mixed oxides with cobalt when oxygen is present, in particular W, Mo, V and Ta, can be detrimental to the H_2 and CO selectivity.

Fig. 3 shows steady-state temperature profiles during catalytic partial oxidation of methane at 15 Nl CH_4/(g h). It illustrates that the addition of Mn, Re and Cr enhanced the combustion activity of the catalyst in the oxidation zone without significantly and adversely affecting the reforming properties of the catalyst, as detailed in the results in Table 2. The addition of Ni, which is known as the commercial choice for a reforming catalyst, did not affect the temperature profile at this low gas velocity.

The most likely explanation for the apparent position of the temperature maximum infront of the catalyst bed is due to catalyst fines sticking to the sides of the reactor wall during filling, which would then be present in the inert layer of alumina. Other less likely explanations include gas-phase combustion, either from back-diffused H_2 or from free radical reactions involving CH_x species. Free radical reactions, however, can be expected to produce C_{2+} species, but this was not observed in the product gas indicating either that they were converted over the catalyst or never produced. With oxygen breakthrough and deactivation the ethane content present in the feed (30–40 ppm) was observed to be unchanged. In support of H_2 back-diffusion, spatially resolved temperature and species profiles reported by Horn et al. [37] indicated some conversion of O_2 to H_2O upstream of a rhodium on alumina foam catalysts, however this was not observed in a follow-up [44].

Fig. 3 illustrates that the gas temperature dropped rapidly through the catalyst bed. This may suggest a multi-step reaction mechanism. Such steps could include pyrolysis, combustion and partial oxidation at the catalyst surface followed by reforming reactions throughout the catalyst bed approximately equilibrating the gas mixture at the bed exit. The fact that the product appears to be equilibrated at the bed-exit gas temperature is in accordance with what has been reported where model simulations were compared to temperature and concentration measurements with high space resolution [37]. The surface temperature at the reactor entrance is, however, typically not equilibrated with the gas temperature [30,32,41,45,46], as was also suggested for our catalysts in Section 3.1.

Figs. 4a–4b illustrate the effect of increasing the gas velocity. Re/Co and Cr/Co deactivated at relatively low GHSVs, while

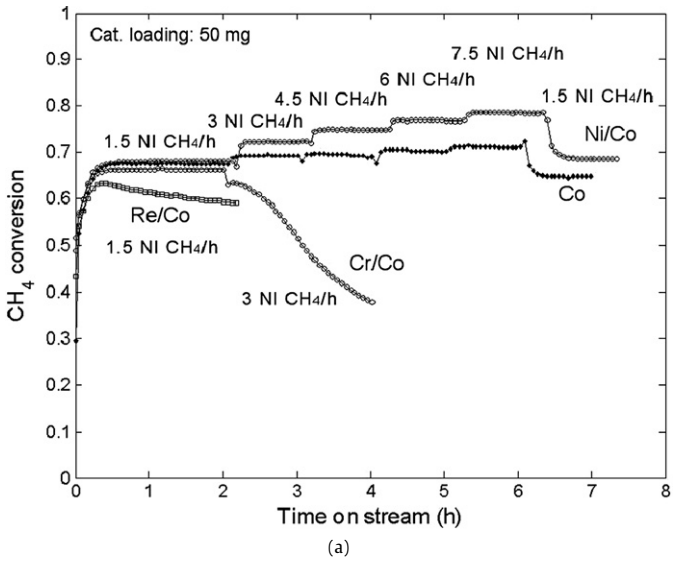

(a)

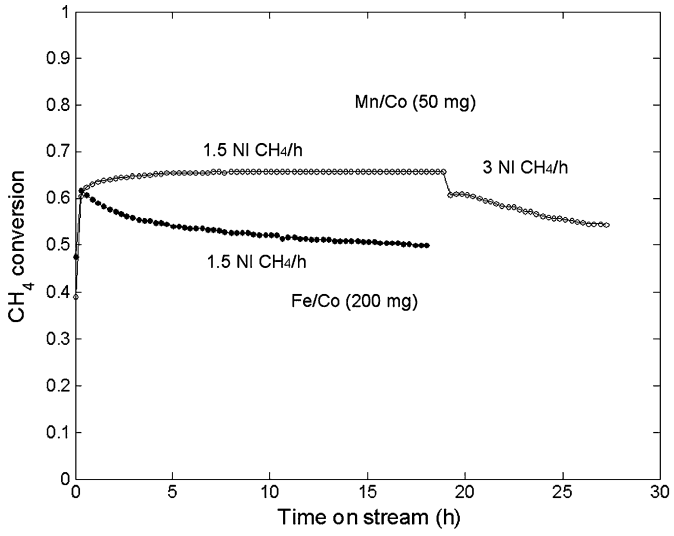

(b)

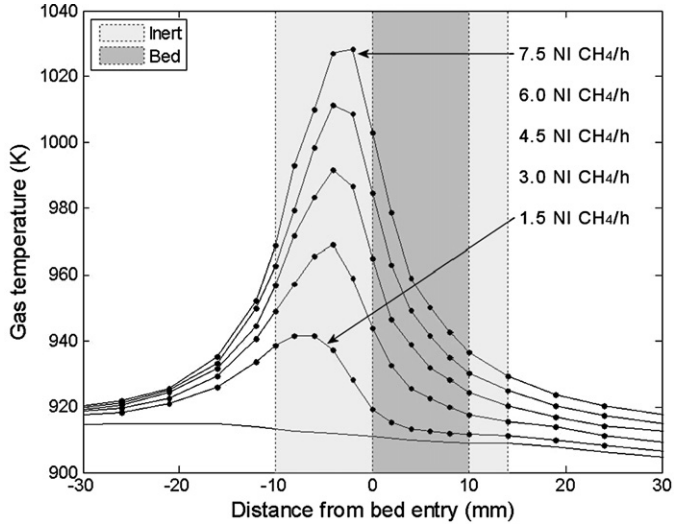

(c)

Fig. 4. Results from the partial oxidation of methane with air (CH_4/O_2 = 2.0) at 923 K (oven temperature) and GHSV = 15–150 Nl CH_4/(g h). Each steady-state was kept for at least 1 h before changing the GHSV. CH_4 conversion levels versus time on-stream for different GHSV's on (a) Co, Ni/Co, Cr/Co and Re/Co, (b) Fe/Co and Mn/Co and (c) gas temperatures as a function of gas velocity for Ni/Co.

pure Co and Ni/Co remained active even at 150 Nl CH_4/(g h). Another extensive study on cobalt catalysts in the partial oxidation of methane, with different reducible promoters at relevant conditions has been published elsewhere [20]. Those results indicated that depending on the support and activity of the promoters, modified cobalt catalysts may remain active at higher GHSVs and at lower temperatures than pure cobalt. However, the low-temperature activity could possibly be heavily affected by the activity of the promoter itself as the nature of the cobalt phase was not investigated *in situ*.

Unmodified Co/α-Al_2O_3 experienced some deactivation at higher GHSVs. This can be seen from the lower conversion level at the end of the run where the gas velocity was returned to the initial value, see Fig. 4a. The Ni/Co catalyst did not experience the same deactivation.

It is believed that cobalt deactivates by surface reoxidation, since it is observed experimentally that it deactivates very rapidly when oxygen breakthrough is observed. It has been reported in literature that Co_3O_4 and Fe_2O_3 activate methane very poorly at lower temperatures when tested at increasing temperatures, but performed better at decreasing temperatures once they were activated [47]. The conclusion is that cobalt is not easily reduced by the interaction of methane with its oxidised surface, but requires pre-reduction to become active for dissociative methane activation. All catalysts tested in this study were pre-reduced. *In situ* TPR was carried out on both active and deactivated Co/α-Al_2O_3 catalysts to further investigate the reason for deactivation. This is discussed in Section 3.5.

Fig. 4b shows that Mn/Co requires a long period of activation before it reaches a conversion level comparable to that of pure Co or Ni/Co, and it deactivated slowly once the gas velocity was increased. The deactivation could possibly be caused by Mn-enhanced reoxidation of the cobalt phase, but carbon formation cannot be ruled out without further investigations. The Fe/Co catalyst deactivated even at low GHSVs, and carbon formation was observed on the used catalyst.

It is suggested that on the catalysts modified with Mo, W, V and Ta, the reducibility of the catalysts was too poor to effectively dissociate methane at the applied conditions. For all these catalysts total combustion was observed to dominate, which correlates to a lack of active sites for methane dissociation and H_2 formation, as indicated by the low H/Co values in Table 2.

3.3. Temperature-programmed cooling during CPO

Figs. 5a–5c show that the product composition at only 15 Nl CH_4/(g h) is approximately equilibrated at the bed exit gas temperature before the catalysts deactivate around 800 K. This deactivation coincides with oxygen breakthrough.

The apparent differences between the conversion levels and selectivities of different catalysts prior to deactivation may be related to variations in actual surface temperatures, as the steady state temperature profiles in Fig. 3 indicated variations in gas temperatures, however, only gas temperatures were measured in this study. Another possibility is that the bed exit gas temperature may have been affected by minor discrepancies, by fractions of a millimetre, in the positioning of the thermocouple. Complicating the temperature measurements, the temperature gradient close to the bed exit increases with decreasing bed exit temperatures, rendering the measurement of actual bed exit temperatures more uncertain as the temperature is decreased.

3.4. Methane activation

The dissociation of methane on freshly reduced cobalt catalysts began around the phase transition temperature (695 K) from hcp

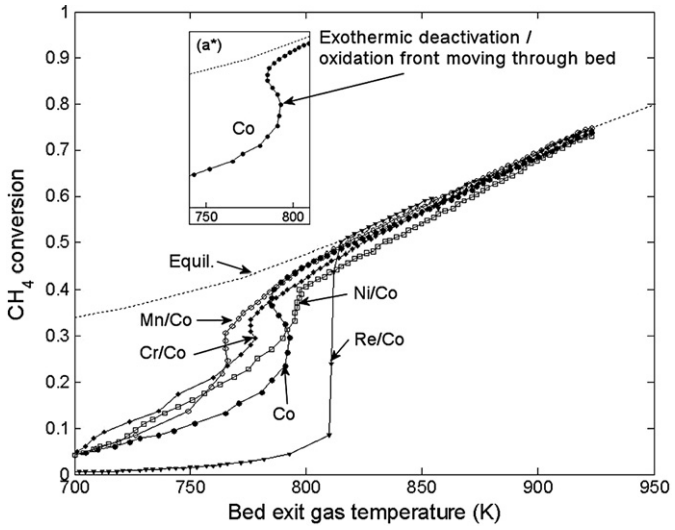

(a)

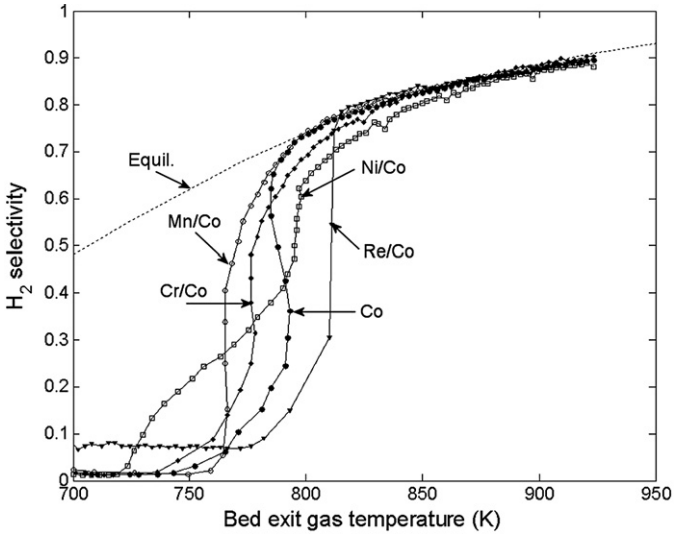

(b)

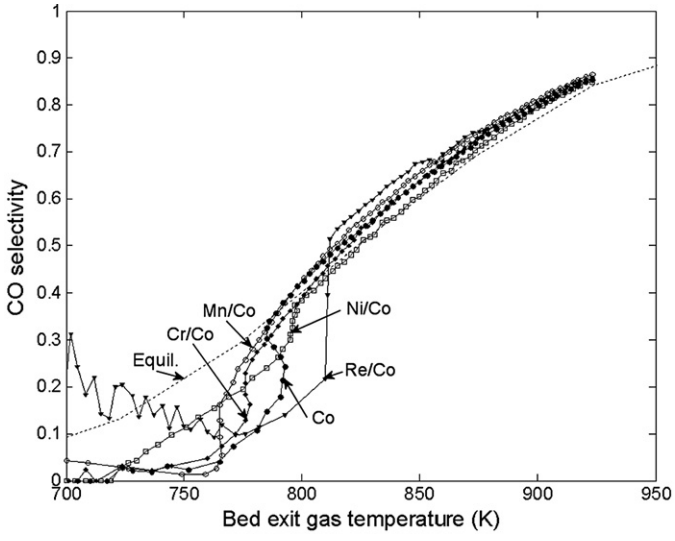

(c)

Fig. 5. Results from the partial oxidation of methane with air (CH_4/O_2 = 2.0) at 923 K (oven temperature) and GHSV = 15 Nl CH_4/(g h). Steady state was kept for 2 h before the oven temperature was decreased with 1 K/min. Results during temperature cooling (−1 K/min) showing (a) CH_4 conversion, (a*) detail illustrating the deactivation of Co/α-Al_2O_3, (b) H_2 selectivity and (c) CO selectivity as functions of the bed exit gas temperature.

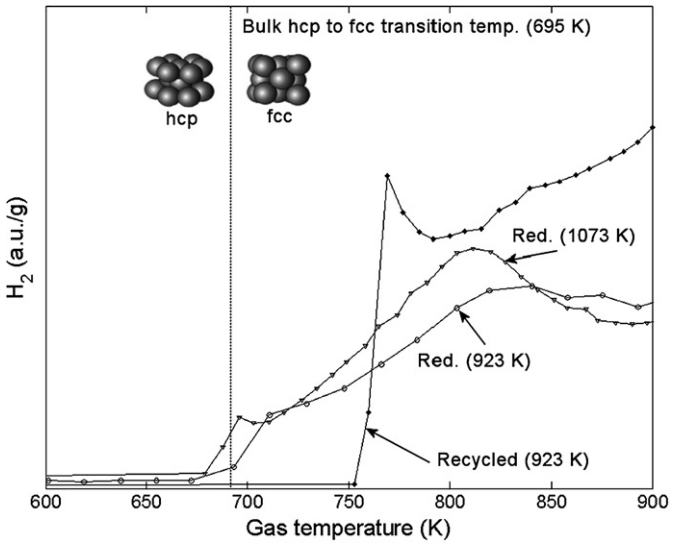

Fig. 6. Temperature-programmed methane dissociation carried out *in situ* using the micro GC, 20 Nml CH_4/min in 500 Nml N_2/min. Temperature was increased from ambient to 1073 K at 5 K/min. (1) 'Red. (923 K)' indicates reduction at 923 K, (2) 'Recycled (923 K)' is run (1) re-reduced at 923 K with subsequent TP-decomposition, (3) 'Red. (1073 K)' indicates reduction at 1073 K.

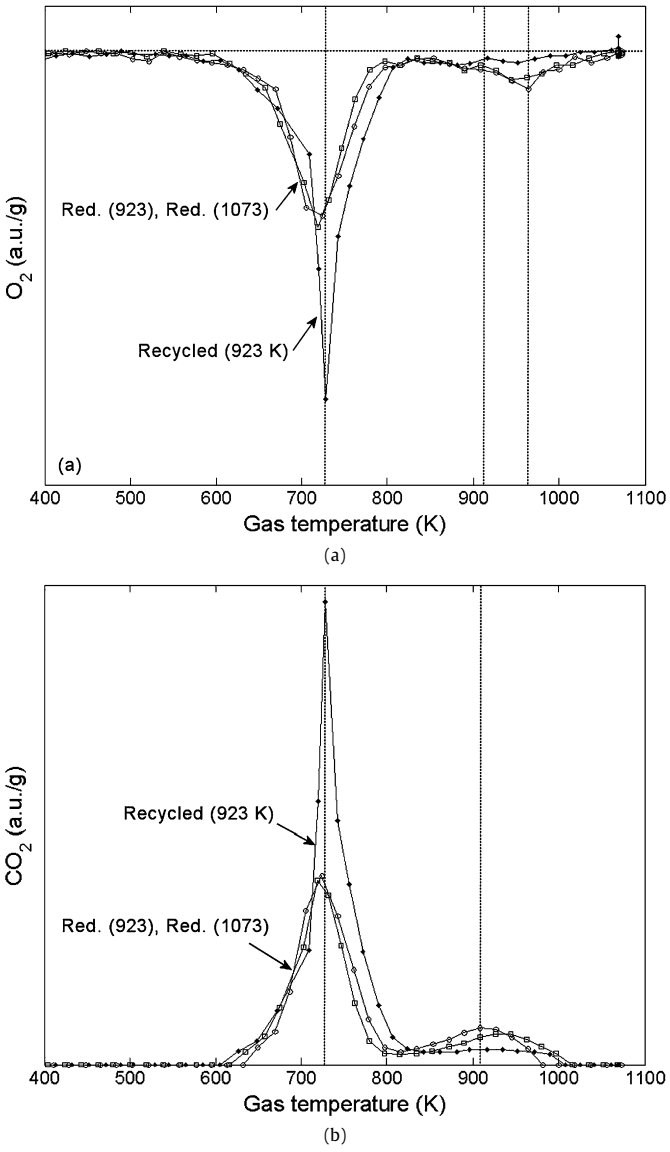

Fig. 7. TPO profiles obtained *in situ* using the micro GC, 50 Nml air/min in 500 Nml N_2/min. Temperature was increased from ambient to 1073 K at 5 K/min. The profiles correlates by name to those in Fig. 6. As functions of the temperature showing (a) O_2 consumption and (b) CO_2 development during TPO.

to fcc structure [48]. All plots from the temperature-programmed methane dissociation at 5 K/min are given in Fig. 6. The subsequent TPOs are given in Figs. 7a and 7b. From the TPOs it follows that carbon is present on the catalyst, and that the combustion of this carbon occurs in two steps where the first begins around 600 K. The presence of two CO_2 peaks could possibly be related to the combustion of multilayer carbon (whisker) followed by the combustion of carbon bound to the surface (graphitic), or it could be that some carbon has been deposited on the support. Another explanation could be differences in Co–C binding energies, in example comparable to those found by Bjørgum et al. [49] on nickel. The second CO_2 peak does not correspond to a large peak in O_2 consumption. There are most likely more than one process occurring, including oxidation of the exposed cobalt particles, and the exact nature of this process requires further studies by *in situ* X-ray absorption fine structure analysis.

The presence of two types of carbon formed during methane dissociation over transition metals (iron, cobalt and nickel) was reported several decades ago by Robertson [50,51]. At that time these two types of carbon was termed single crystal graphite and polycrystalline non-graphitic carbon (filamentous carbon). Dissociation of methane has later been studied in order to grow filamentous carbon nanotubes [52,53]. Avdeeva et al. [52] reported fcc cobalt structure from XRD analysis of the passivated used catalyst, where the catalyst had been used for methane dissociation and carbon growth. The temperature-programmed dissociation measurements reported in this paper is consequently in line with literature.

Fig. 6 shows that the recycled catalyst required higher temperatures to activate methane during temperature-programmed methane dissociation. This could indicate changes in the surface morphology of the catalyst. Higher carbon formation could be related to seeds for carbon growth remaining on the recycled catalyst. This is suggested by the increased formation of CO_2 in Fig. 7b.

3.5. Catalyst deactivation

The deactivation process observed during temperature cooling has already been illustrated in Fig. 5a, where the conversion of methane was plotted as a function of bed exit temperatures. Based on Fig. 5a* the deactivation of Co/α-Al_2O_3 can be interpreted to involve a heat wave from the oxidation zone which moves through the bed upon deactivation. This coincides with oxygen breakthrough and corresponding changes in the selectivities.

As already mentioned, bulk cobalt metal changes its structure from hcp to fcc at 690–695 K [48], but the cobalt catalysts deactivated rapidly before this limit was reached, as illustrated in Figs. 5a–5c. It is therefore unlikely that the deactivation of cobalt is in any way related to such metallic phase transition.

To further investigate the deactivation process, *in situ* TPR was obtained for both active and deactivated Co/α-Al_2O_3 catalysts. The results are given in Fig. 8. The TPR profile labeled 'TPO-TPR' was obtained on a catalyst first oxidised by TPO which was not tested in CPO. The three other signals were obtained for catalysts tested in the partial oxidation using 30 Nl CH_4/(g h). One after 2 h steady-state at 988 K ('TPR-988'), a second during temperature cooling before deactivation at 833 K ('TPR-833'), and the third after complete deactivation for synthesis gas formation at 773 K ('TPR-773').

Fig. 8 indicates that deactivation is associated with reoxidation of the active phase, and that the working catalyst is only partially reduced. The profile labeled 'TPR-773', which was obtained

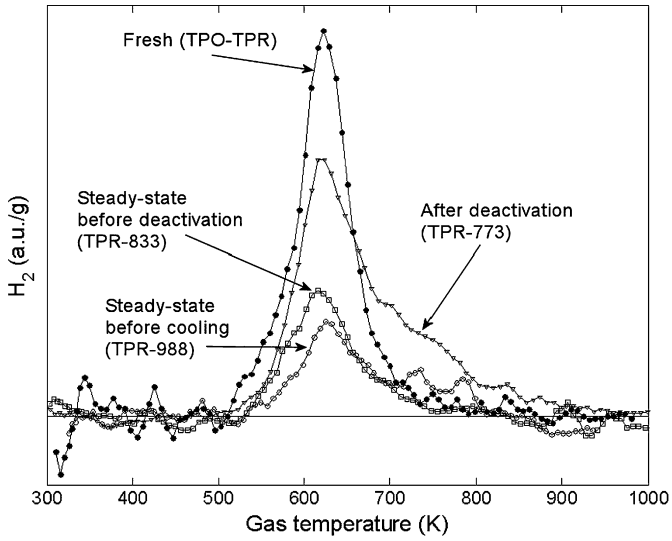

Fig. 8. TPR profiles obtained *in situ* using the micro GC, 10 Nml H_2/min in 500 Nml N_2/min. Temperature was increased from ambient to 973 K at 5 K/min. 'TPO-TPR' was obtained on a catalyst first oxidised by TPO which was not tested in CPO. The three other signals were obtained for catalysts tested in the partial oxidation using 30 Nl CH_4/(g h). 'TPR-988' after 2 h steady-state at 988 K, 'TPR-833' after temperature cooling before deactivation at 833 K, and 'TPR-773' after complete deactivation for synthesis gas formation at 773 K.

after deactivation, has a shoulder that is not found on the catalysts investigated after steady-state operation or after temperature cooling before deactivation. Such shoulders are commonly observed in TPR measurements, and when extending beyond the temperature range of the two-step cobalt reduction process, these are typically related to small particles with strong support interactions, ranging from small metal oxides to surface spinels and bulk spinels (>1050 K).

Effects on the deactivation relating to carbon deposition was not investigated. The literature [54,55] suggests that carbon deposition over cobalt catalysts is a much smaller problem than over nickel, in fact, cobalt has successfully been added to nickel catalysts to reduce carbon deposition [54]. Nishimoto et al. [55] suggested different reaction pathways on cobalt and nickel to explain the high resistance to carbon deposition on cobalt. Another explanation for the promoter effect observed when adding cobalt to nickel could be an increased dispersion of nickel, creating smaller ensembles such that the structure sensitive growth of carbon filaments [56,57] is inhibited. However, dispersion measurements which could elucidate this has not yet been reported.

3.6. Adsorption properties

The reason for carrying out H_2 chemisorption measurements was to clarify whether reduced metallic species are present when the catalyst is exposed to a reducing atmosphere. It is known that dissociative methane activation and H_2 formation requires metallic sites when investigating nickel catalysts [58,59]. Furthermore, it was expected that the intrinsic formation of H_2 as well as the reforming properties of the catalyst would depend on its available metal surface area.

The calculated H/Co adsorption ratios in Table 1 correspond to the metal dispersion if there is no contribution from the second metal and it is assumed that the adsorption stoichiometry on cobalt is H/Co = 1.0 [60]. Small contributions from the second metal can in general not be excluded on the basis of simple chemisorption measurements, but based on thermodynamic considerations only nickel is suspected to have yielded species present in its zero valent state.

It is therefore more likely that the large variations in the measured adsorption ratio H/Co reflects the effect of the second metal/metal oxide by covering a fraction of the cobalt surface, or by inducing an increased oxidation state of Co. This view is supported by Scherrer thickness calculations from the XRD spectra of Co^0. The cobalt particles were all in the range 15–18 nm, indicating comparable dispersions. It could be suggested that the second metal or metal oxide would reduce the available cobalt surface area by blocking pore entrances, but the measurements of volumetric adsorption of nitrogen given in Table 2 do not indicate any pore blocking. This view is further supported by the XPS measurements where surface enrichment of the promoter relative to cobalt is observed. See Section 3.9 for further details on the XPS measurements.

According to the metal phase diagrams of relevant bimetallic species, Co–Ni and Co–Re are completely miscible in the temperature range relevant to this study. Co–Cr may form a variety of different phases, while Co–Mo forms an intermediate phase with a Co/Mo ratio of about 1. W, V and Ta are known to form bimetallic compounds with Co with M/Co ratio of about 1/3, i.e. Co_3M or Co_7M_2. However, based on thermodynamic calculations using the software HSC CHEMISTRY 5.1, it is believed that most of the modifiers were oxidised at the conditions applied during methane partial oxidation.

3.7. X-ray diffraction

Table 1 summarizes XRD results giving estimates for Co^0 particle sizes. In addition to zero valent cobalt, CoO peaks were observed on the Cr/Co and Mn/Co catalysts corresponding to particle sizes of 7.6 ± 0.5 nm and 5.5 ± 0.7 nm, respectively. If CoO was present on the other samples it was undetectable indicating crystallite sizes <2–3 nm. Other detected peaks were $CoWO_4$ (21.0 ± 0.8 nm) and TaO_2 (31.6 ± 3.7 nm).

Assuming spherical particles and the approximation that the diameter of a spherical particle is about 1.25 times that of the Scherrer thickness, $d = 1.25t$ [61], the dispersion of the catalyst can be estimated using Eq. (9),

$$D\% = \frac{96.2}{1.25t}, \tag{9}$$

and the Scherrer thickness obtained from XRD [62,63]. It follows that the dispersion for all samples in this study is in the range 4.3–5.2% using XRD, which does not correlate well with the H_2 chemisorption experiments. These apparent discrepancies in dispersion values are most likely caused by surface layers of modifier oxide or selective poisoning of chemisorption sites. This is discussed further in Section 3.9 on XPS,

It cannot be ruled out that some of the discrepancies in dispersion values for the modified catalysts as compared to the unmodified catalyst could be related to larger crystallite clusters on the modified catalysts, as schematically illustrated in Fig. 9b as compared to Fig. 9a. However, it is unlikely that this is the main reason when comparing the different modified catalysts. Fig. 9c illustrates a case where the dispersion from XRD is most correct, and where a modifier is covering the cobalt crystallites effectively blocking chemisorption sites. The true picture is most likely a combination of Figs. 9b and 9c.

3.8. Temperature-programmed reduction/oxidation

Figs. 10a and 10b illustrate TPR profiles of both oxidised catalysts (solid lines), and directly reduced catalyst precursors subsequently exposed to air at room temperature before TPR (stippled lines).

The stippled lines are composed of two distinct features. There is a peak at lower temperatures, in the range 500–700 K, and on

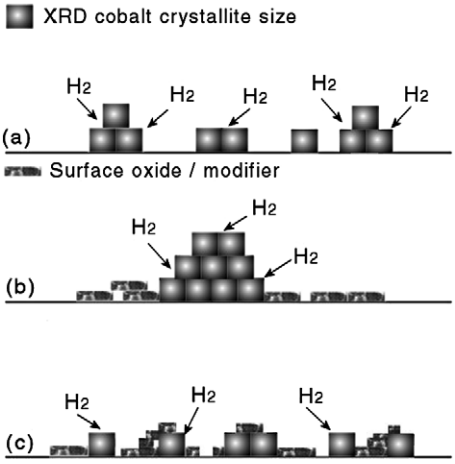

Fig. 9. Illustration of how crystallite clusters affect the measured dispersion value $D(\mathrm{XRD})$ or $D(\mathrm{H_2})$. A dispersion value calculated on the basis of cobalt crystallite size from XRD does not account for the effect of crystallite clusters. XRD and H_2 dispersion values are comparable when no clusters are present. (a) High dispersion with some small clusters, $D(\mathrm{XRD}) > D(\mathrm{H_2})$, (b) low dispersion with large clusters, but no surface oxide layers, $D(\mathrm{XRD}) \gg D(\mathrm{H_2})$ and (c) high dispersion with surface oxide layers, $D(\mathrm{XRD}) \gg D(\mathrm{H_2})$.

some catalysts there is also a peak at higher temperatures, in the range 900–1100 K. These peaks are most likely related to the following properties:

The low-temperature peaks can either be related to the reduction of cobalt nitrate, which is known to occur in two steps in the range 500–700 K [64], or they can be related to surface-reoxidised species. If the peaks are related to cobalt nitrate, the shifts seen in the low temperature peak when comparing different TPR profiles could indicate the degree of availability of nitrate species to the reducing agent (hydrogen). If the peaks are related to oxygen species, the shifts and splits could indicate different coordination numbers of oxygen for the surface-reoxidised species. Only elemental analysis on nitrogen could clarify further whether these species are cobalt precursors or surface oxygen species. In either case these species were not observed with XRD. The effect of calcination temperature and atmosphere on residual nitrate was investigated by Borg et al. [65]. Significantly less residual nitrate is typically observed on α-Al_2O_3 supports as compared to γ-Al_2O_3 [66]. Considering the thermodynamic stability of cobalt metal exposed to air, it is expected that some degree of reoxidation has occurred, supporting the view that the low temperature peaks are at least partially related to surface-reoxidised species or chemisorbed oxygen.

The high-temperature peaks are related to highly dispersed CoO, with the exception of the W/Co catalyst where $CoWO_4$ was observed with XRD. On Cr/Co and Mn/Co there were observed CoO crystallites with XRD, while this was not detectable on the other catalysts, most likely due to a higher dispersion and consequently smaller particle sizes. Very small high-temperature peaks were observed for all catalysts.

Since TaO_2 was observed with XRD, this phase appears to be very difficult to reduce since no clear TPR peak is found. This observation is supported by thermodynamic calculations using HSC Chemistry 5.1.

Following the first TPR (stippled lines) the catalysts were completely oxidised by TPO. Since the support was calcined at a high temperature (1398 K), it was possible to do this without the formation of bulk spinel structures that might otherwise occur in metal-alumina systems exposed to O_2 at elevated temperatures. If present this would be observable as a peak in the range 1100–1200 K, but no such peak was detected.

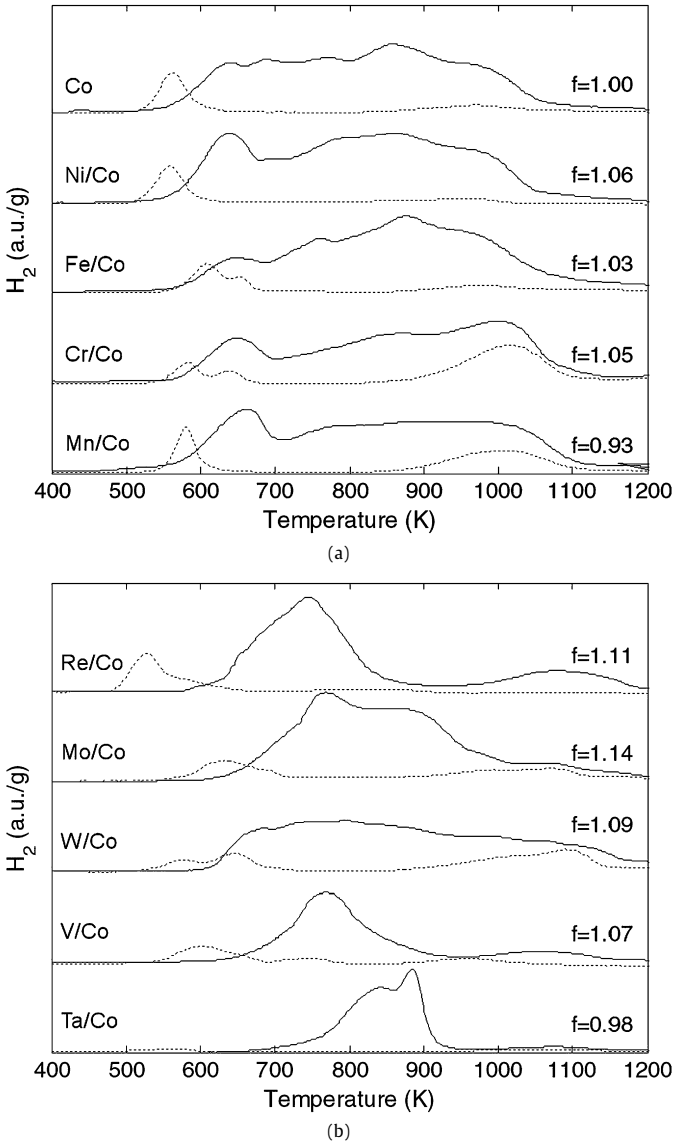

Fig. 10. TPR profiles obtained at 10 K/min. Dotted lines represents TPR signals of fresh catalysts. Solid lines are TPR signals after TPO. f correlates the area under each TPR curve relative to the unmodified Co catalyst. $f \leqslant 1.00$ indicate a catalyst which is more difficult to reduce, while $f > 1.00$ indicate either additional reduction of MO_x and/or promoted reduction of Co. The uncertainty in f is about ± 0.02. The TCD signals were scaled to force fit all samples in the same figure. (a) Diagrams for Co, Ni/Co, Fe/Co, Cr/Co and Mn/Co, and (b) diagrams for Re/Co, Mo/Co, W/Co, V/Co and Ta/Co.

All catalysts, with the exception of V/Co and Ta/Co, oxidised at approximately the same rate during TPO. When compared to Co/α-Al_2O_3, the TPO peak on V/Co and Ta/Co were shifted to higher temperatures by 55 K and 135 K, respectively, which could indicate poor availability of metallic cobalt exposed to the oxidizing agent (oxygen) on these samples. This is in accordance with the chemisorption results. Several catalysts exhibited shoulders suggesting the oxidation of different species or different oxidation states.

The TPR plots shown by the solid lines in Figs. 10a and 10b were obtained after TPO and focusing on the first maxima it can be seen how the reduction of Co^{2+} shifts depending on the modifying species.

The TPR profiles were reproducible. The variations in H_2 consumption, or the TPR fine structure, is most likely related to different CoO_x species, their particle sizes and support interactions.

Table 3
XPS analysis results.

	Co_{2p_3}	Cr_{2p_3}	Mo_{d_3}	Ta_{4d_3}	Ta_{4d_5}	V_{2p}	W_{4d_3}	W_{4d_5}
X/Co_{2p_3} [a]	1.00	0.27	0.70	0.84	0.90	1.24	0.79	0.98
$(X + Co_{2p_3})/Al_{2s}$	0.029	0.050	0.088	0.024	0.025	0.113	0.112	0.116

[a] X here represents the peaks i.e. Co_{2p_3} or Cr_{2p_3}, etc.

On the modified samples the CoO_x–MO_x interactions are likely to have contributed, where M is the second metal, and the different contributions in this fingerprint method are therefore not possible to identify without additional structure sensitive information being obtained simultaneously. The following prominent features of the TPO-TPR catalysts are worth noting:

The addition of Cr appears to exert a negative effect on the overall degree of reduction of cobalt. This could either be related to the numerous possible Co–Cr phases observed in the bimetallic phase diagram [67], which could have formed during preparation, or the presence of strong CoO_x–CrO_y interactions.

The Ta modified catalyst is by far the most difficult catalyst to initiate the reduction of, and as noted earlier also the most difficult catalyst to oxidise after the reduction of catalyst precursors.

3.9. X-ray photoelectron spectroscopy

The results from XPS investigations on some of the catalysts are given in Table 3. For the catalysts promoted with V and Ta the XPS measurements were especially important in order to elucidate the surface properties of the catalysts since chemisorption of H_2 failed to yield any dispersion value.

Comparing the values for X/Co_{2p_3} all samples that were unsuccessful in converting methane to synthesis gas (see Table 2) have a X/Co_{2p_3} ratio 2–4 higher than Cr/Co, which yielded equilibrium conversion and selectivity. The fact that the impregnated ratio of X/Co was 1/15 indicates that in all cases the available surface is enriched with the modifier. This surface enrichment can either indicate a higher dispersion of the second phase, or it can indicate the formation of surface layers on cobalt, bimetallic or mixed oxide species with cobalt. In any case it is observed that Mo, Ta, V and W decrease the available surface area of cobalt as compared to Cr, which is in line with the chemisorption experiments.

Comparing the values for $(X + Co_{2p_3})/Al_{2s}$ the support signal on the sample with Ta is much higher as compared to the other samples. The support signal is actually comparable to the unmodified cobalt sample, which could indicate either that Ta had a large negative effect on the Co dispersion or that Ta-species are in intimate contact with cobalt either as bimetallic species or more likely as surface oxide layers. The XRD measurements indicated that the cobalt crystallites were perhaps slightly larger on Ta/Co as compared to the other modified samples, but the results using the Scherrer thickness equation and peak mapping were not conclusive in this respect. Consequently the formation of surface layers of TaO_2, a phase which was observed in XRD, appears to be the best explanation.

The $(X + Co_{2p_3})/Al_{2s}$ values for Cr, Mo, V and W modified catalysts are higher than for the pure cobalt catalyst, indicating either that the dispersion of cobalt is increased or that the second phase contributes to cover the support. The chemisorption values, however, indicate reduced available cobalt surface area with modification, which does not speak in favour of an increased dispersion. The XRD results also support this view. It is therefore more likely that the second element is highly dispersed, most likely as an oxide and at least to a some degree on the support.

Because the XPS signal resolution was rather low with only 20 passes of a large spectrum, it was not possible to investigate chemical shifts in detail, but XRD and TPx have already testified the presence of mostly Co^0 and small amounts of Co^{2+}. All the signals were, however, observed to shift in the XPS spectrum. Table 4 gives the peak positions of Co_{2p_3}, C_{1s} and Al_{2s}. By comparing the positions of these peaks in the catalysts Cr/Co, Mo/Co, Ta/Co, V/Co and W/Co relative to the unmodified Co catalyst, all these peaks were shifted by the same amount of energy. The C_{1s} signal is the background signal from the carbon paper pads on which the catalyst samples were mounted, and it is consequently not part of the catalyst itself, although contamination from organic materials are usually present yielding a clear C_{1s} signal. This signal should therefore not shift in the spectrum depending on the catalyst investigated. Hence it is concluded that these shifts are caused by sample charging. According to [68] the binding energies of Co_{2p_3}, C_{1s} and Al_{2s} are 781.9 (or 778.4 eV for Co^0), 284.7 and 119.9 eV, respectively. Based on this it is calculated that all samples experienced charging to the extent of 5–15 eV.

Table 4
XPS peak positions (eV) and charging shifts.

	Co	CoCr	CoMo	CoTa	CoV	CoW
Co_{2p_3}	793.4	793.4	794.8	795.6	787.4	798.2
C_{1s}	297.8	298.0	299.0	300.2	291.6	302.8
Al_{2s}	132.0	131.8	133.4	134.2	125.8	137.6
[a] ΔCo_{2p_3}	0.0	0.0	1.4	2.2	−6.0	5.0
ΔC_{1s}	0.0	0.2	1.2	2.2	−6.2	5.0
ΔAl_{2s}	0.0	−0.2	1.4	2.4	−6.2	5.6

[a] The Δ here compares the signals of CoX to Co, i.e. ΔCo_{2p_3} for CoTa and Co is $795.6 - 793.4 = 2.2$.

4. Conclusions

Different modified cobalt catalysts were investigated in the partial oxidation of methane using air as oxidant with $CH_4/O_2 = 2$. The reaction was most likely affected by diffusional limitations on heat and mass transport, and the product composition appeared to be limited by global thermodynamics. Any deviation away from equilibrium could be explained by temperature gradients.

The presence of a modifying species that forms oxides at conditions relevant to methane partial oxidation, in particular elements with less than 5 *d*-electrons on the highest level, such as W, V and Ta are especially detrimental to catalyst performance. Fe is also not very suitable in catalytic partial oxidation of methane, both because of its propensity to be oxidised and because it promotes the formation of carbon deposits.

XPS measurements indicated that the surface was enriched with modifier, and that this modifier to some degree covered the support surface around the cobalt particles. However, from combining XPS with H_2 chemisorption and XRD measurements the results strongly indicated selective poisoning or partial coverage of the cobalt particles by the modifier. The presence and possible effects of bimetallic species could not be excluded based on the reported investigations.

Using *in situ* temperature-programmed methods the activation of methane and catalyst deactivation were investigated over Co/α-Al_2O_3. C–H bond activation was found to occur around the hcp to fcc phase transition temperature of cobalt, and deactivation of cobalt catalysts in catalytic partial oxidation of methane appeared to involve reoxidation of the active phase.

Acknowledgments

The financial supports of the Research Council of Norway, and StatoilHydro through the RENERGI program, and the Norwegian University of Science and Technology (NTNU) are greatly acknowledged. The authors are grateful to S. Raaen at the department of physics at NTNU for obtaining the XPS spectra.

References

[1] M.A. Peña, J.P. Gómez, J.L.G. Fierro, Appl. Catal. A 144 (1996) 7.
[2] J.N. Armor, Appl. Catal. A 176 (1999) 159.
[3] P. Ferreira-Aparicio, M.J. Benito, J.L. Sanz, Catal. Rev. Sci. Eng. 47 (2005) 491.
[4] C. Song, Catal. Today 115 (2006) 2.
[5] S. Freni, G. Calogero, S. Cavallaro, J. Power Sources 87 (2000) 28.
[6] H. Liander, Trans. Faraday Soc. 25 (1929) 462.
[7] M. Prettre, C. Eichner, M. Perrin, Trans. Faraday Soc. 42 (1946) 335b.
[8] A.T. Ashcroft, A.K. Cheetham, J.S. Foord, M.L.H. Green, C.P. Grey, A.J. Murrell, P.D.F. Vernon, Nature 344 (1990) 319.
[9] A.T. Ashcroft, A.K. Cheetham, M.L.H. Green, P.D.F. Vernon, Nature 352 (1991) 225.
[10] D.A. Hickman, L.D. Schmidt, Science 259 (1993) 343.
[11] S.S. Bharadwaj, L.D. Schmidt, Fuel Process. Technol. 42 (1995) 109.
[12] S.C. Tsang, J.B. Claridge, M.L.H. Green, Catal. Today 23 (1995) 3.
[13] A.P.E. York, T. Xiao, M.L.H. Green, Top. Catal. 22 (2003) 345.
[14] Q. Zhu, X. Zhao, Y. Deng, J. Nat. Gas. Chem. 13 (2004) 191.
[15] Y.H. Hu, E. Ruckenstein, Adv. Catal. 48 (2004) 297.
[16] A.P.E. York, T.-C. Xiao, M.L.H. Green, J.B. Claridge, Catal. Rev. Sci. Eng. 49 (2007) 511.
[17] B.C. Enger, R. Lødeng, A. Holmen, Appl. Catal. A 346 (2008) 1.
[18] D.A. Hickman, L.D. Schmidt, J. Catal. 138 (1992) 267.
[19] P.A. Schweitzer, Metallic Materials—Physical, Mechanical, and Corrosion Properties, Marcel Dekker, New York, 2003.
[20] R. Lødeng, E. Bjørgum, B.C. Enger, J.L. Eilertsen, A. Holmen, B. Krogh, M. Rønnekleiv, E. Rytter, Appl. Catal. A 333 (2007) 11.
[21] S. Tang, J. Lin, K.L. Tan, Catal. Lett. 59 (1999) 129.
[22] L. Mo, X. Zheng, C. Huang, J. Fei, Catal. Lett. 80 (2002) 165.
[23] L. Mo, J. Fei, C. Huang, X. Zheng, J. Mol. Catal. A Chem. 193 (2003) 177.
[24] Q. Miao, G. Xiong, S. Sheng, W. Cui, L. Xu, X. Guo, Appl. Catal. A 154 (1997) 17.
[25] S. Brunauer, P.H. Emmett, E. Teller, J. Am. Chem. Soc. 60 (1938) 309.
[26] E.P. Barrett, L.G. Joyner, P.P. Halenda, J. Am. Chem. Soc. 73 (1951) 373.
[27] E. Blekkan, A. Holmen, S. Vada, Acta Chem. Scand. 47 (1992) 275.
[28] H. Klug, L. Alexander, X-Ray Diffraction Procedures for Polycrystalline and Amorphous Materials, Wiley, New York, 1954.
[29] F. Basile, G. Fornasari, F. Trifirò, A. Vaccari, Catal. Today 64 (2001) 21.
[30] B. Li, S. Kado, Y. Mukainakano, M. Nurunnabi, T. Miyao, S. Naito, K. Kunimori, K. Tomishige, Appl. Catal. A 304 (2006) 62.
[31] F. Basile, G. Fornasari, F. Trifirò, A. Vaccari, Catal. Today 77 (2002) 215.
[32] B. Li, K. Maruyama, M. Nurunnabi, K. Kunimori, K. Tomishige, Appl. Catal. A 275 (2004) 157.
[33] L. Basini, A. Guarinoni, A. Aragno, J. Catal. 190 (2000) 284.
[34] L. Basini, K. Aasberg-Petersen, A. Guarinoni, M. Østberg, Catal. Today 64 (2001) 9.
[35] P.B. Weisz, C.D. Prater, Adv. Catal. 6 (1954) 143.
[36] D.E. Mears, Ind. Eng. Chem. Process Des. Dev. 10 (1971) 541.
[37] R. Horn, K.A. Williams, N.J. Degenstein, L.D. Schmidt, J. Catal. 242 (2006) 92.
[38] R. Horn, K.A. Williams, N.J. Degenstein, L.D. Schmidt, Chem. Eng. Sci. 62 (2007) 1298.
[39] D. Dalle Nogare, N.J. Degenstein, R. Horn, P. Canu, L.D. Schmidt, J. Catal. 258 (2008) 131.
[40] G.F. Froment, K.B. Bischoff, Chemical Reactor Analysis and Design, Wiley, New York, 1990.
[41] M. Bizzi, L. Basini, G. Saracco, V. Specchia, Chem. Eng. J. 90 (2002) 97.
[42] Y.-F. Chang, H. Heinemann, Catal. Lett. 21 (1993) 215.
[43] J.-D. Grundwaldt, S. Hannemann, C.G. Schroer, A. Baiker, J. Phys. Chem. B 110 (2006) 8674.
[44] R. Horn, K.A. Williams, N.J. Degenstein, A. Bitsch-Larsen, D. Dalle Nogare, S.A. Tupy, L.D. Schmidt, J. Catal. 249 (2007) 380.
[45] B. Li, R. Watanabe, K. Maruyama, M. Nurunnabi, K. Kunimori, K. Tomishige, Appl. Catal. A 290 (2005) 36.
[46] B. Li, R. Watanabe, K. Maruyama, K. Kunimori, K. Tomishige, Catal. Today 104 (2005) 7.
[47] Å. Slagtern, H.M. Swaan, U. Olsbye, I.M. Dahl, C. Mirodatos, Catal. Today 46 (1998) 107.
[48] Properties and Selection: Nonferrous Alloys and Special-Purpose Materials—Pure Metals, ASM Handbooks Online, vol. 2, ASM International, 2003.
[49] E. Bjørgum, D. Chen, M.G. Bakken, K.O. Christensen, A. Holmen, J. Phys. Chem. B 109 (2005) 2360.
[50] S.D. Robertson, Carbon 8 (1970) 365.
[51] S. Robertson, Carbon 10 (1972) 221.
[52] L.B. Avdeeva, D.I. Kochubey, S.K. Shaikhutdinov, Appl. Catal. A 177 (1999) 43.
[53] S.-P. Chai, S.H. Sharif Zein, A.R. Mohamed, Chem. Phys. Lett. 426 (2006) 345.
[54] V.R. Choudhary, A.M. Rajput, B. Prabhakar, A.S. Mamman, Fuel 77 (1998) 1803.
[55] H.-A. Nishimoto, K. Nakagawa, N.-O. Ikenaga, M. Nishitani-Gamo, T. Ando, T. Suzuki, Appl. Catal. A 264 (2004) 65.
[56] H.S. Bengaard, J.K. Nørskov, J. Sehested, B.S. Clausen, L.P. Nielsen, A.M. Molenbroek, J.R. Rostrup-Nielsen, J. Catal. 209 (2002) 365.
[57] K.O. Christensen, D. Chen, R. Lødeng, A. Holmen, Appl. Catal. A 314 (2006) 9.
[58] C. Li, C. Yu, S. Shen, Catal. Lett. 67 (2000) 139.
[59] C. Li, C. Yu, S. Shen, Catal. Lett. 75 (2001) 183.
[60] R.C. Reuel, C.H. Bartholomew, J. Catal. 85 (1984) 63.
[61] J. Lemaitre, P. Menon, F. Delannay, in: F. Delannay (Ed.), Characterization of Heterogeneous Catalysts, in: Chemical Industries Series, vol. 15, Marcel Dekker Inc., New York, 1984.
[62] R.C. Reuel, C.H. Bartholomew, J. Catal. 85 (1984) 78.
[63] R.D. Jones, C.H. Bartholomew, Appl. Catal. 39 (1988) 77.
[64] M.P. Rosynek, A. Polansky, Appl. Catal. 73 (1991) 97.
[65] Ø. Borg, E.A. Blekkan, S. Eri, D. Akporiaye, B. Vigerust, E. Rytter, A. Holmen, Top. Catal. 45 (2007) 39.
[66] Ø. Borg, M. Rønning, S. Storsæter, W. van Beek, A. Holmen, Stud. Surf. Sci. Catal. 163 (2007) 255.
[67] Alloy Phase Diagrams—Binary Phase Diagrams, ASM Handbooks Online, vol. 3, ASM International, 2003.
[68] B.V. Crist, Handbook of Monochromatic XPS Spectra. The Elements of Native Oxides, Wiley, New York, 2000.